

RESEARCH ARTICLE

10.1002/2017GC006822

Rock record and magnetic response to large earthquakes within Wenchuan Earthquake Fault Scientific Drilling cores

Lei Zhang^{1,2}, Zhiming Sun¹ , Haibing Li³ , Laishi Zhao², Sheng-Rong Song⁴, Yu-Min Chou⁵, Yong Cao^{1,6} , Xiaozhou Ye¹, Huan Wang³, and Xiangli He⁶

Key Points:

- Twenty-one layers of pseudotachylytes occur from 579.62 to 599.31 m-depth within WFSD-2 cores
- Neoformented magnetite in pseudotachylytes contributes to the higher values of magnetic susceptibility in WFSD-2 cores
- Powerful seismic events have occurred repeatedly in the Longmen Shan thrust belt

Supporting Information:

- Supporting Information S1

Correspondence to:

Z. Sun,
sunzm1209@163.com

Citation:

Zhang, L., Z. Sun, H. Li, L. Zhao, S.-R. Song, Y.-M. Chou, Y. Cao, X. Ye, H. Wang, and X. He (2017), Rock record and magnetic response to large earthquakes within Wenchuan Earthquake Fault Scientific Drilling cores, *Geochem. Geophys. Geosyst.*, 18, 1889–1906, doi:10.1002/2017GC006822.

Received 23 JAN 2017

Accepted 6 APR 2017

Accepted article online 12 APR 2017

Published online 10 MAY 2017

© 2017. The Authors.

This is an open access article under the terms of the Creative Commons Attribution-NonCommercial-NoDerivs License, which permits use and distribution in any medium, provided the original work is properly cited, the use is non-commercial and no modifications or adaptations are made.

¹Key Laboratory of Paleomagnetism and Tectonic Reconstruction of Ministry of Land and Resources, Institute of Geomechanics, Chinese Academy of Geological Sciences, Beijing, China, ²China University of Geosciences (Wuhan), Wuhan, China, ³Institute of Geology, Chinese Academy of Geological Sciences, Beijing, China, ⁴Department of Geosciences, National Taiwan University, Taipei, Taiwan, ⁵Department of Ocean Science and Engineering, South University of Science and Technology, Shenzhen, China, ⁶China University of Geosciences (Beijing), Beijing, China

Abstract Fault-related pseudotachylytes are often considered to be produced by large seismic events. To investigate the rock record and magnetic response to large earthquakes within cores from the Wenchuan Earthquake Fault Scientific Drilling borehole 2 (WFSD-2), we carried out microstructural, geochemical, and rock-magnetic analyses of representative cores. Based on microstructural observations and powder X-ray diffraction analyses, we found 21 layers of melt-origin pseudotachylytes from 579.62 to 599.31 m-depth in the cores. The presence of early-formed pseudotachylyte fragments in the new layer suggests that seismic faulting processes exploited the same fault strand more than once. Pseudotachylyte veins have higher values of magnetic susceptibility relative to wall rocks. Rock-magnetic results indicate that the magnetic minerals within the pseudotachylyte veins are magnetite with varying amounts of paramagnetic minerals. Magnetic hysteresis loops show that a reduction of the grain size of ferromagnetic minerals is not a plausible explanation for the higher magnetic susceptibility values in pseudotachylyte veins. Rock-magnetic analyses indicate that frictional heating (>500°C) occurred in the pseudotachylyte veins during large earthquakes. The resulting high temperatures induced thermal decomposition of paramagnetic minerals, forming magnetite and contributing to the higher magnetic susceptibility values. Different generations of pseudotachylytes and numerous high magnetic susceptibility zones together demonstrate that ancient powerful earthquakes may have occurred repeatedly in the Longmen Shan thrust belt.

1. Introduction

Knowledge of the microstructural, physical, and chemical properties of fault rocks in seismogenic zones is important for understanding the mechanism of powerful seismic faulting events [Chester, 1995; Chester and Chester, 1998; Biegel and Sammis, 2004; Faulkner et al., 2008]. Previous studies indicate that pseudotachylytes, fault gouge, and gouge graphitization are geological records of seismic fault slip [Sibson, 1975; Magloughlin, 1992; Di Toro and Pennacchioni, 2004; Andersen and Austrheim, 2006; Lin, 2008; Li et al., 2013; Kuo et al., 2014]. In addition, frictional heating within a fault zone may cause the physical and chemical alteration of the magnetic mineral assemblages within the host rocks [Nakamura et al., 2002; Chou et al., 2012a; Ferré et al., 2012]. Consequently, rock-magnetic properties of fault rocks can provide important information about frictional heating in earthquake slip zones [Mishima et al., 2006, 2009]. Previous magnetic studies of pseudotachylytes and gouge have revealed the occurrence of positive magnetic susceptibility anomalies compared to the protolith, implying that new magnetic minerals were formed during frictional heating [Nakamura and Iyeda, 2005; Ferré et al., 2005, 2012; Hirono et al., 2006a, 2006b; Tanikawa et al., 2008]. Therefore, positive magnetic susceptibility anomalies in gouge and pseudotachylytes may constitute evidence of large earthquakes. The rock magnetism of fault rocks can be used to estimate the frictional heating temperature in a fault zone. For example, the formation of ferromagnetic maghemite or magnetite by thermal decomposition of paramagnetic phases indicates that the disk-shaped black materials within samples from TCDP Hole B experienced temperatures of at least 400°C [Mishima et al., 2006]. Magnetic studies conducted by Chou et al. [2012b]

indicated that pyrrhotite probably formed at high temperatures ($>500^{\circ}\text{C}$) at the expense of pyrite in gouge within the principal slip zone of the Chi-Chi earthquake. These studies indicate that rock magnetism can potentially detect frictional heating in earthquake slip zones.

The Longmen Shan thrust belt has long been active and has experienced large earthquakes [Li *et al.*, 2006; Densmore *et al.*, 2007; Li *et al.*, 2008]. During the Wenchuan earthquake (Mw 7.9, 2008), two surface ruptures occurred along the Anxian-Guanxian and Yingxiu-Beichuan faults [Li *et al.*, 2008]. To investigate the physical properties in large displacements of the ruptured faults and the mechanism of the Wenchuan earthquake faulting, the Wenchuan Earthquake Fault Scientific Drilling (WFSD) was initiated immediately after the Wenchuan earthquake [Xu *et al.*, 2008]. Microstructural, geochemical, and geophysical studies from surface ruptures and WFSD cores demonstrate that the pseudotachylytes, fresh fault gouge, and gouge graphitization constitute rock records of powerful earthquakes [Kuo *et al.*, 2014; Li *et al.*, 2014, 2016; Wang *et al.*, 2015]. However, the only outcrop of pseudotachylyte in the Longmen Shan thrust belt was found in the Pengguan Complex along the Yingxiu-Beichuan fault [Pei *et al.*, 2014a; Wang *et al.*, 2015; Zheng *et al.*, 2016]. The presence of pseudotachylytes within WFSD cores has been not reported until now.

Rock-magnetic studies of the surface rupture zones and WFSD cores have revealed positive magnetic susceptibility anomalies in pseudotachylyte veins and fault gouge [Yang *et al.*, 2013, 2016; Pei *et al.*, 2014a, 2014b; Li *et al.*, 2016; Zhang *et al.*, 2017]. The main reason for the high values of magnetic susceptibility in fault rocks may be the neoformation of ferromagnetic minerals during a large earthquake [Yang *et al.*, 2012a; Liu *et al.*, 2016]. A preliminary rock-magnetic study of the Jiulong outcrops across the Anxian-Guanxian fault indicated that the frictional heating may be less than 300°C [Liu *et al.*, 2014]. Liu *et al.* [2016] reported that possible magnetic transformations resulted from the neoformation of magnetite at high temperatures ($>500^{\circ}\text{C}$) during the large earthquake in the Yingxiu-Beichuan fault. Wang *et al.* [2015] concluded that temperatures reached as high as 1730°C in the Bajiaomiao outcrop based on the microstructural characteristics of pseudotachylyte. However, the temperature of frictional heating in the fault rocks within the Longmen Shan thrust belt is still debated, and in addition rock-magnetic studies of fault rocks (especially pseudotachylyte) obtained directly from borehole cores of WFSD are lacking.

Here we present the results of a study of the microstructure, geochemistry, and magnetic properties of pseudotachylyte veins and wall rocks within WFSD-2 cores. Our aims are to better understand the rock record and magnetic resonance signal produced by large earthquakes and to estimate the temperature of frictional heating during an earthquake.

2. Geological Setting

The NE-SW-trending Longmen Shan thrust belt is located between the Sichuan Basin and the eastern margin of the Tibetan Plateau and is characterized by a steep topographic gradient and a high topographic relief of 3000–4500 m [Densmore *et al.*, 2007]. The Longmen Shan thrust belt, which is approximately 500 km long and 30–60 km wide, is mainly composed of three thrust faults: the Anxian-Guanxian, Yingxiu-Beichuan, and Wenchuan-Maoxian faults, from SE to NW (Figure 1) [Li *et al.*, 2006]. The Wenchuan earthquake produced 80 and 270 km coseismic surface rupture zones along the Anxian-Guanxian and Yingxiu-Beichuan faults, respectively (Figure 1) [Li *et al.*, 2008].

The second hole (WFSD-2) was drilled in Bajiaomiao village, Hongkou County (Dujiangyan, Sichuan Province), on the hanging wall of the Yingxiu-Beichuan fault (YBF) (Figure 1) [Zhang *et al.*, 2012]. The WFSD-2 cores comprise seven rock units: the Pengguan Complex (0–599.31, 1211.49–1360.25, 1361.26–1679.51, and 1715.49–2081.47 m-depth) and the Triassic Xujiahe Formation (599.31–1211.49, 1679.51–1715.48, and 2081.47–2283.56 m-depth) [Zhang *et al.*, 2017]. The Pengguan Complex is the result of Neoproterozoic activity and mainly consists of plagiogranite, biotite granite, granodiorite, tonalite, intermediate-acidic intrusive rocks similar to diorite, and various mafic-ultramafic intrusive rocks, volcanics, and pyroclastic rocks [Li *et al.*, 2013]. Based on Sibson's [1977] fault-rock classification, Zhang *et al.* [2012] reported that the predominant fault rocks in the WFSD-2 borehole cores are cataclasite, ultracataclasite, fault breccia, and fault gouge. The present study focuses on the Pengguan Complex from 565.53 to 599.31 m-depth, composed of granodiorite (565.53–579.62 m) and a cataclasite zone (579.62–599.31 m).

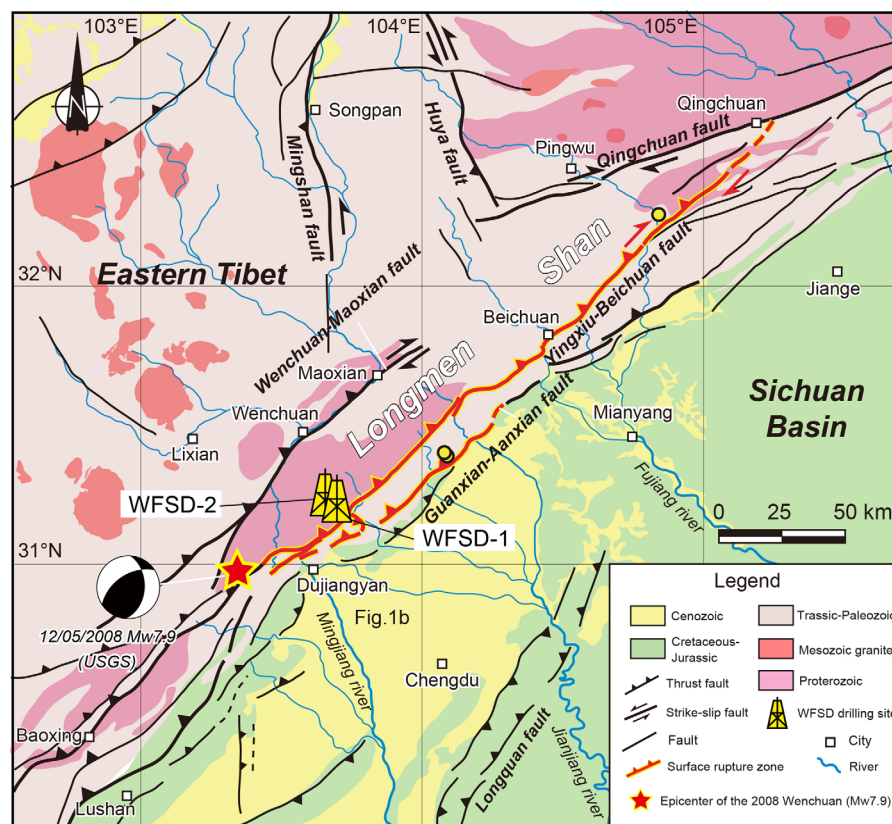


Figure 1. Geological map of the Longmen Shan thrust belt, modified from *Li et al.* [2014]. Also shown is the site of the WFSD-2 borehole. WFSD-2 was drilled along the YBF, 300 m northwest of WFSD-1, to a final depth of 2283.56 m.

3. Sampling and Methods

3.1. Sampling

The studied cataclasite zone within the WFSD-2 cores is from 579.62 to 599.31 m (Figure 2a). The wall rock of the cataclasite unit is granodiorite (Figure 2b). The veins, including gray veins and dark veins, are exposed in the cataclasite zone (Figure 2). Twenty-one layers of veins are observed in the cataclasite zone (Figure A in the supporting information). We sampled the cataclasite zone from 579.62 to 599.31 m-depth in the WFSD-2 cores (Figures 2c and 2e–2h), and the wall rock at different depths (Figure 2b). Three different rock types, including veins, cataclasite, and granodiorite, were chosen for analysis (Table 1). The magnetic susceptibility of the cores was measured from the cataclasite zone and wall rock (565.53–566.13 and 579.50–599.31 m-depth). Twenty-eight samples (S1–S28) were obtained from the WFSD-2 cores (Figure 2 and Table 1). Six power samples of pseudotachylyte (S11, S19, S24, S26, S27, and S28) were carefully removed using a small diamond drill bit with an optical magnifying glass. Twelve powder samples were chosen for powder X-ray diffraction (XRD) measurements; 8 samples were selected for magnetic hysteresis measurements; 9 powder samples were selected for low-temperature magnetic measurements; and 16 cylindrical samples were used for measurement of the thermal demagnetization of three-component isothermal remanent magnetization (IRM). The cylindrical solid samples were obtained using an electric drill with a 1 cm-diameter drill pipe. However, the thin pseudotachylyte veins in WFSD-2 cores are generally injected into cataclasites and therefore, it was difficult for us to collect cores of whole pseudotachylyte veins. Thus, these solid samples from pseudotachylyte veins may include material from the surrounding clasts. In addition, three powder samples were selected for measurement of K-T curves.

3.2. Methods

An optical microscope and Scanning Electron Microscope (SEM) were used for microstructural analyses of cataclasite and dark veins. Microscope observations were made at various magnifications using an Olympus

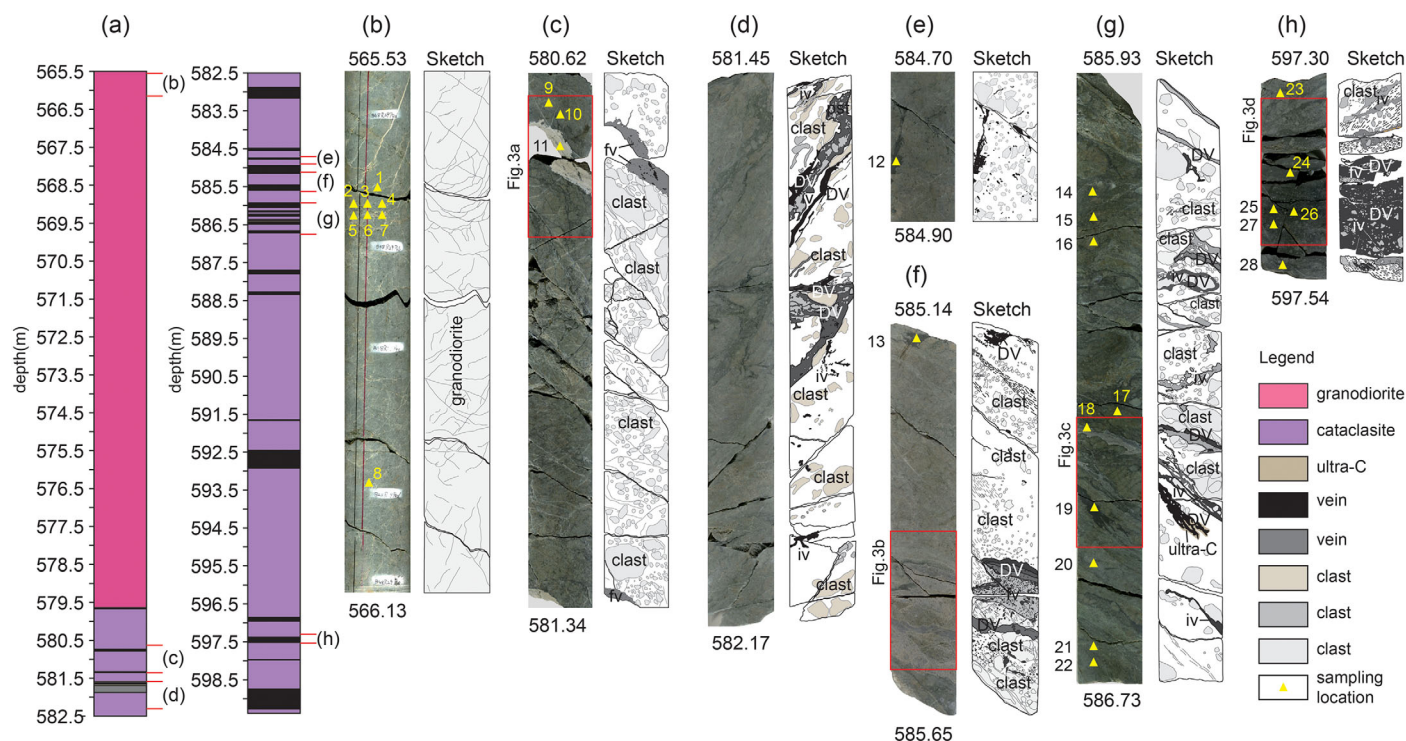


Figure 2. Illustrations of representative cores from the cataclasite zone and the wall rock within WFSD-2 cores, with sampling locations. (a) Lithology chart from 565.50 to 599.31 m-depth. (b) 565.53–566.13 m-depth: granodiorite with thin quartz veins. (c) 580.62–581.34 m-depth: gray fault veins that appear as planar veins; black veins injected into gray veins; rounded-to-subangular clasts orientated by flow structures. (d) 581.45–582.17 m-depth: black network veins showing complex morphology. (e) 584.70–584.90 m-depth: dark vein injected into cataclasite. (f) 585.14–585.65 m-depth: different-colored vein lays with sharp contact and subangular-to-rounded clasts orientated by flow structure. (g) 585.93–586.73 m-depth: black, dark-gray, and gray layers of veins, with the same orientation. (h) 597.30–597.54 m-depth: thick injection veins and fault veins. ultra-C: ultracataclasite; DV: dark vein; iv: injection vein; fv: fault vein; red rectangle: the location of Figure 3.

BX51 optical microscope, at the Institute of Geology, Chinese Academy of Geological Sciences, Beijing. SEM images were obtained using a LEO Stereoscan 440 SEM equipped with EDX at Taiwan University in Taipei. The SEM was operated at 15 keV with a 4 nA current.

Powder X-ray diffraction (XRD) analyses can be used to confirm the crystalline phase(s) present in a sample [Loubser and Verryn, 2008]. The mineral compositions of the samples were determined by XRD analyses at the Micro Structure Analytical Laboratory in Peking University. XRD patterns were determined using a Dmax 12 kW powder diffractometer (CuK α) at 40 kV and 100 mA, with a scanning rate of 4° min⁻¹ and a sampling width of 0.02°, and 0°–70° (2 θ).

Magnetic susceptibility was measured at a 5 mm interval using a Bartington MS2E sensor incorporated in the Multi Sensor Core Logger in the Institute of Geology, Chinese Academy of Geological Sciences, Beijing. The sensing region of the MS2E sensor is at the end of a 25 mm diameter ceramic cylinder mounted in line with the electronics unit and comprises a 10.5 × 3.8 mm rectangular surface. The frequency of the MS2E sensor is 2 kHz, and the sensitivity is 1 × 10⁻⁶ SI.

Magnetic hysteresis loops were measured in the physics laboratory of Peking University using a Princeton alternating gradient force magnetometer (Model 2900 AGM), with 1 T maximum applied field. Saturation remanence (M_{rs}), saturation magnetization (M_s), and coercivity (H_c) were obtained after subtracting the paramagnetic contribution.

Low-temperature isothermal remanence measurements of representative samples were made using a Quantum Design Magnetic Property Measurement System (MPMS XP-5, sensitivity = 5.0 × 10⁻¹⁰ A m²) at the State Key Laboratory of Lithospheric Evolution, Institute of Geology and Geophysics, Chinese Academy of Sciences, Beijing. Field-cooled (FC) and zero-field-cooled (ZFC) curves were measured by cooling samples from 300 to 20 K in a 2.0 T field and zero field, respectively, followed by imparting an SIRM in a 2.0 T field

Table 1. Lithology, Location of Samples, and Measurements^a

Number	Sample	Lithology	Depth (m)	Measurements
1	S1	Granodiorite	565.80	XRD, magnetic hysteresis loops, MPMS, K-T
2	S2	Granodiorite	565.82	IRM
3	S3	Granodiorite	565.82	IRM
4	S4	Granodiorite	565.82	IRM
5	S5	Granodiorite	565.84	IRM
6	S6	Granodiorite	565.84	IRM
7	S7	Granodiorite	565.84	IRM
8	S8	Granodiorite	566.05	XRD, MPMS
9	S9	Cataclasite	580.68	XRD, MPMS
10	S10	Cataclasite	580.70	XRD, MPMS, K-T
11	S11	Gray vein	580.72	XRD, magnetic hysteresis loops
12	S12	Dark vein	584.82	IRM
13	S13	Dark vein	585.15	IRM
14	S14	Cataclasite	586.06	IRM
15	S15	Cataclasite	586.08	IRM
16	S16	Cataclasite	586.14	IRM
17	S17	Cataclasite	586.37	XRD, magnetic hysteresis loops, MPMS
18	S18	Gray vein	586.40	IRM
19	S19	Dark vein	586.51	XRD, MPMS, K-T
20	S20	Cataclasite	586.60	IRM
21	S21	Cataclasite	586.70	IRM
22	S22	Cataclasite	586.71	IRM
23	S23	Cataclasite	597.34	XRD, magnetic hysteresis loops
24	S24	Dark vein	597.47	XRD, magnetic hysteresis loops, MPMS
25	S25	Dark vein	597.48	IRM
26	S26	Dark vein	597.49	XRD, magnetic hysteresis loops, MPMS
27	S27	Dark vein	597.51	XRD, magnetic hysteresis loops
28	S28	Dark vein	597.53	XRD, magnetic hysteresis loops, MPMS

^aXRD: powder X-ray diffraction; MPMS: magnetic property measurement system; K-T: high-temperature thermomagnetism; IRM: the thermal demagnetization of three-component isothermal remanent magnetization.

and then measuring the remanence in zero field during warming to 300 K. Decay of the remanence was monitored during warming of the sample from 20 to 300 K, at intervals of 5 K.

Magnetic susceptibility-versus-temperature (K-T) curves and thermal demagnetization of three-component IRMs were measured at the Key Laboratory of Paleomagnetism and Tectonic Reconstruction of the Ministry of Land and Resources, Institute of Geomechanics, Chinese Academy of Geological Sciences, Beijing. Thermal demagnetization of three-component IRMs was conducted by exposing the sample to hard (1.2 T), moderate (0.4 T), and weak (0.12 T) magnetic fields sequentially along three orthogonal axes, following *Lowrie* [1990]. Then, all samples were subjected to stepwise (18 steps) thermal demagnetization in an ASC TD-48 oven with an internal residual field of less than 10 nT. Thermomagnetic analysis was performed using a MLY-4S Kappabridge coupled with a CS-4 high-temperature furnace in an air atmosphere, from room temperature to 700°C, with subsequent cooling to room temperature. The average heating and cooling rates were about 7.5°C/min. The K-T curves are listed in the supporting information.

4. Macroscopic Structure and Microstructure of the Cataclasite Zone

4.1. Macroscopic Structure

The cataclastic rock zone consists of veins, cataclasites, and a few ultracataclasites (Figures 2 and 3). Cataclasites are present as the wall rocks. Ultracataclasites are closely related to dark veins (Figures 2f and 3c). Cataclasites are grayish in color in the WFSD-2 cores (Figures 2c–2f and 3a–3c). The clasts in the cataclasite are mainly subangular-to-subrounded and the sizes range from n mm to n cm. The veins are stiffer and more cohesive than cataclasite and comprise injection veins and fault veins. The injection veins, as networks and individual veins, have a complex and irregular morphology (Figures 3a and 3c). The fault veins, evident as planar veins along the fault, are several mm to ~5 cm in thickness (Figures 3a and 3b). The thick veins generally contain subangular-to-subrounded fragments in a dark aphanitic matrix with flow structures (Figures 3a, 3b, and 3d). The fragments mainly comprise cataclastic clast aggregates consisting of quartz and plagioclase fragments. In addition, fragments of black vein are injected into the gray vein (Figure 3a). The veins appear gray (Figures 2c and 3a), dark-gray (Figures 2f and 3c), brown (Figures 2e and 3b), and black (Figures 2d, 2f, 2g, 3b, and 3d) in macroscopic view. Twenty-one layers of veins with different colors and thicknesses can be observed in the cataclasite zone (supporting information Figure A). The veins range from n mm to n

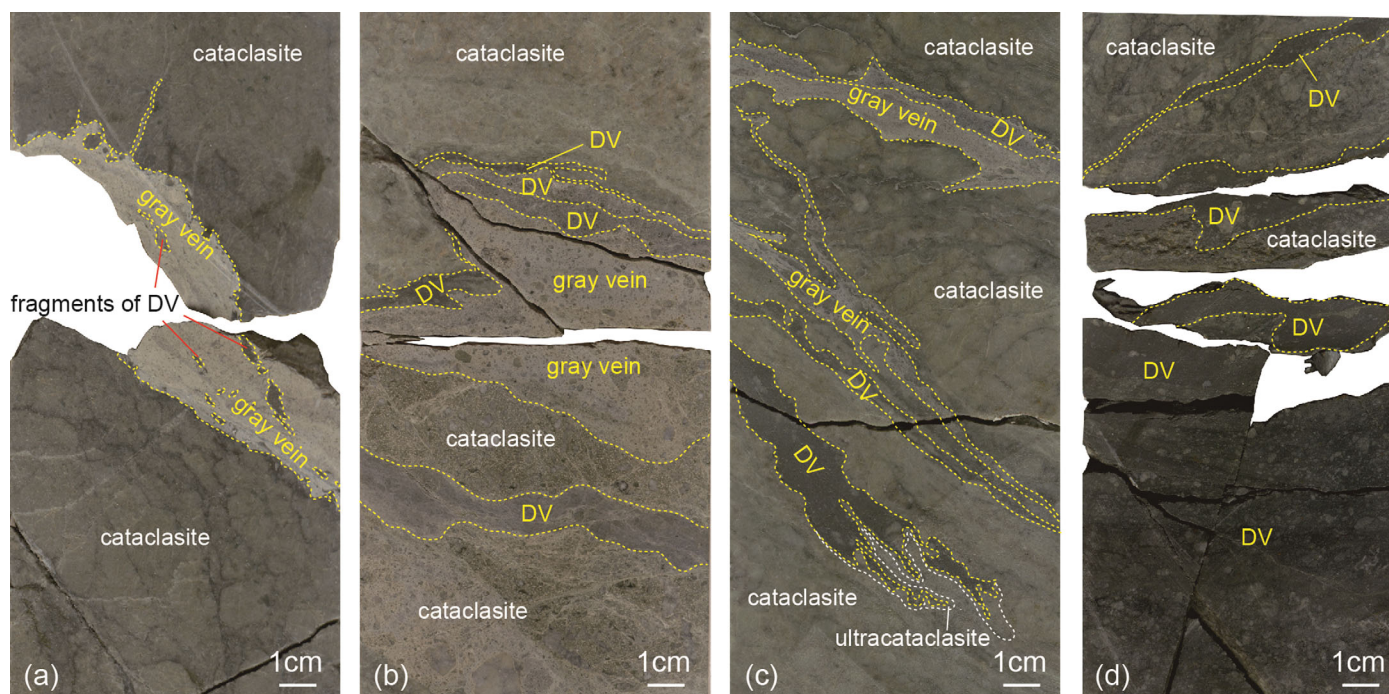


Figure 3. Photographs illustrating the presence of veins in the cataclasite zone within WFSD-2. (a) 580.65–580.83 m-depth: gray vein injected into cataclasite as a flame; fragments of black vein injected into gray vein. (b) 585.41–585.59 m-depth: different-colored vein lays with sharp contact. (c) 586.38–586.56 m-depth: black, dark-gray, and gray layers of veins. Black vein injected into cataclasite as a root; ultracataclasite is associated with black veins. (d) 597.32–597.50 m-depth: thick veins injected into cataclasite with no clear boundary. DV: dark vein.

cm in width. Some veins injected into cataclasites exhibit sharp boundaries (supporting information Figures Aa–Ai and Ak), while others lack clear boundaries (supporting information Figures Ah, Aj, and Al–Ap).

4.2. Microstructure

Cataclasite usually consists of 50–90% clasts by volume. The clasts are scattered in a fine-grained matrix and consist of feldspar, quartz, and calcite of various shapes, including embayed, rounded, and other irregular outlines (Figures 4a, 4b, and 4d). The clast size varies widely, from 1 mm to several micrometers. The dark-gray layers associated with cataclasite and dark veins are ultracataclasite (Figure 4a). The ultracataclasite matrix includes quartz and feldspar clasts. The clasts in ultracataclasite are smaller and rounder than in cataclasite and comprise <20% by volume (Figure 4a).

The contacts between the veins and cataclasite are typically sharp but may locally be highly irregular (Figures 4a, 4b, and 4d). The veins appear gray, dark-gray, brown, and black in macroscopic view, while they are evident as dark material under the optical microscope. Different stages of veins are evident as different color tones under the optical microscope (Figures 4b–4d). New dark veins are injected into the old dark veins, and the contacts are also sharp (Figure 4b). Figure 4c shows an example of a dark vein (DV-3) cutting off one clast from another dark vein (DV-4). Dark veins consist of a dark matrix and many fragments of different sizes, varying from nanometers to centimeters. The fragments in the matrix consist of feldspar and quartz and have various shapes such as rounded (Figures 4b and 4d), embayed (Figure 4f), and other irregular outlines (Figure 4c). Flow structures are also observed in dark veins (Figures 4c and 4d); they typically exhibit matrix layers of contrasting colors, streaks curved around the fragments, and oriented clasts. Acicular microlites are visible in dark veins (Figure 4e). Stellate aggregate microlites are composed of thin acicular branches.

The SEM images of the vein from 580.72 m-depth reveal circular spherulites <2 μm in diameter that are well developed between the quartz grains (Figures 5a and 5b). SEM-EDX results indicate that the chemical components of the spherulites are mainly feldspar (Figure 5e). Zoning structures are developed in the large spherulites (Figure 5b), and typical melting textures flowing from the edge of feldspar grains are also observed (Figure 5c). Numerous vesicles with a diameter of about 1 μm and well-rounded quartz grains are observed (Figure 5d); the embayed (Figure 5b) and rounded (Figure 5d) quartz grains indicate that they have been melted. Overall, these findings indicate that the veins are melted.

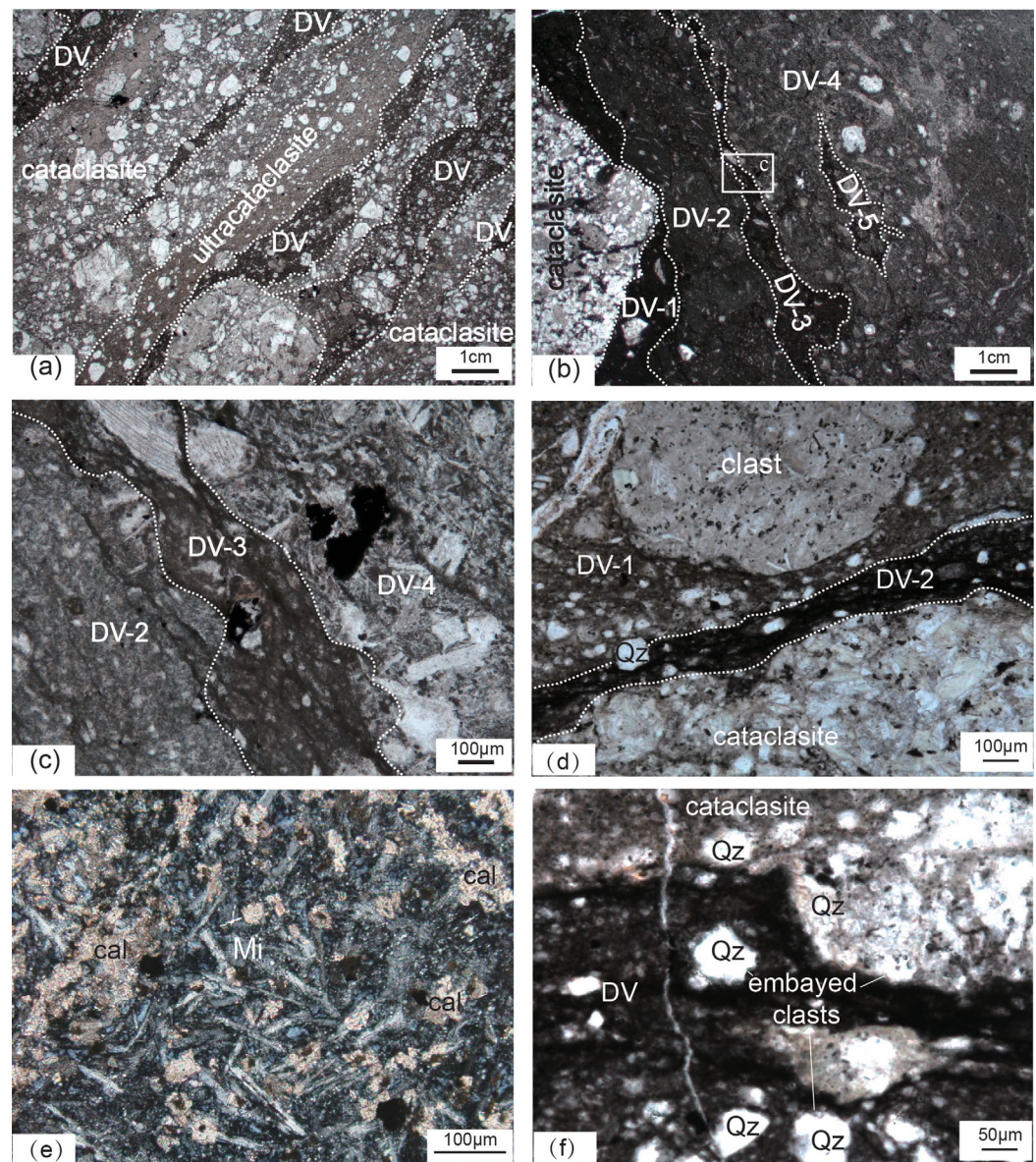


Figure 4. Photomicrographs showing the microstructural features of dark veins. (a) 586.51 m-depth: sharp contacts between cataclasite and dark veins; dark veins injected into cataclasite and ultracataclasite. The dark-gray layer is ultracataclasite. (b) 580.72 m-depth: different stages of dark veins. The boundaries between the dark veins are typically sharp but locally can be highly irregular. Early-formed dark vein fragments are visible in a newly formed dark vein. (c) Enlarged view of the square in Figure 4b, illustrating clear flow structures and different layers of dark vein. DV-3 cutting off one clast from DV-4. (d) 597.47 m-depth: flowing structures and a rounded clast are identified in the two stages of dark veins. (e) 597.47 m-depth: textures of microlite in a dark vein. Stellate aggregate microlites are composed of thin acicular and lath. (f) 597.49 m-depth: embayed quartz fragments showing partial melting structures. DV: dark vein; Qz: quartz; cal: calcite; Mi: microlite; DV-1, DV-2, DV-3, DV-4, and DV-5 indicate different stages of dark veins.

4.3. Powder X-Ray Diffraction

The results of XRD analyses of the granodiorite, cataclasite, and veins from the WFSD-2 cores are listed in Table 2 (supporting information data in Table A). The XRD profiles yield mineral compositions of quartz, albite, calcite, and clay minerals (Figure 6). The granodiorite and cataclasite mainly contain muscovite, quartz, calcite, and albite, and the veins mainly contain muscovite, quartz, kaolinite, and albite. The samples of granodiorite and cataclasite contain a small quantity of clay minerals; in addition, the types of clay minerals differ from those in the veins.

Powder X-ray diffraction patterns can be used to confirm the occurrence of a glassy matrix and fresh glass [Lin, 1994, 2008; Lin and Shimamoto, 1998]. The crystal shows sharp peaks in these spectra (Figure 6). There

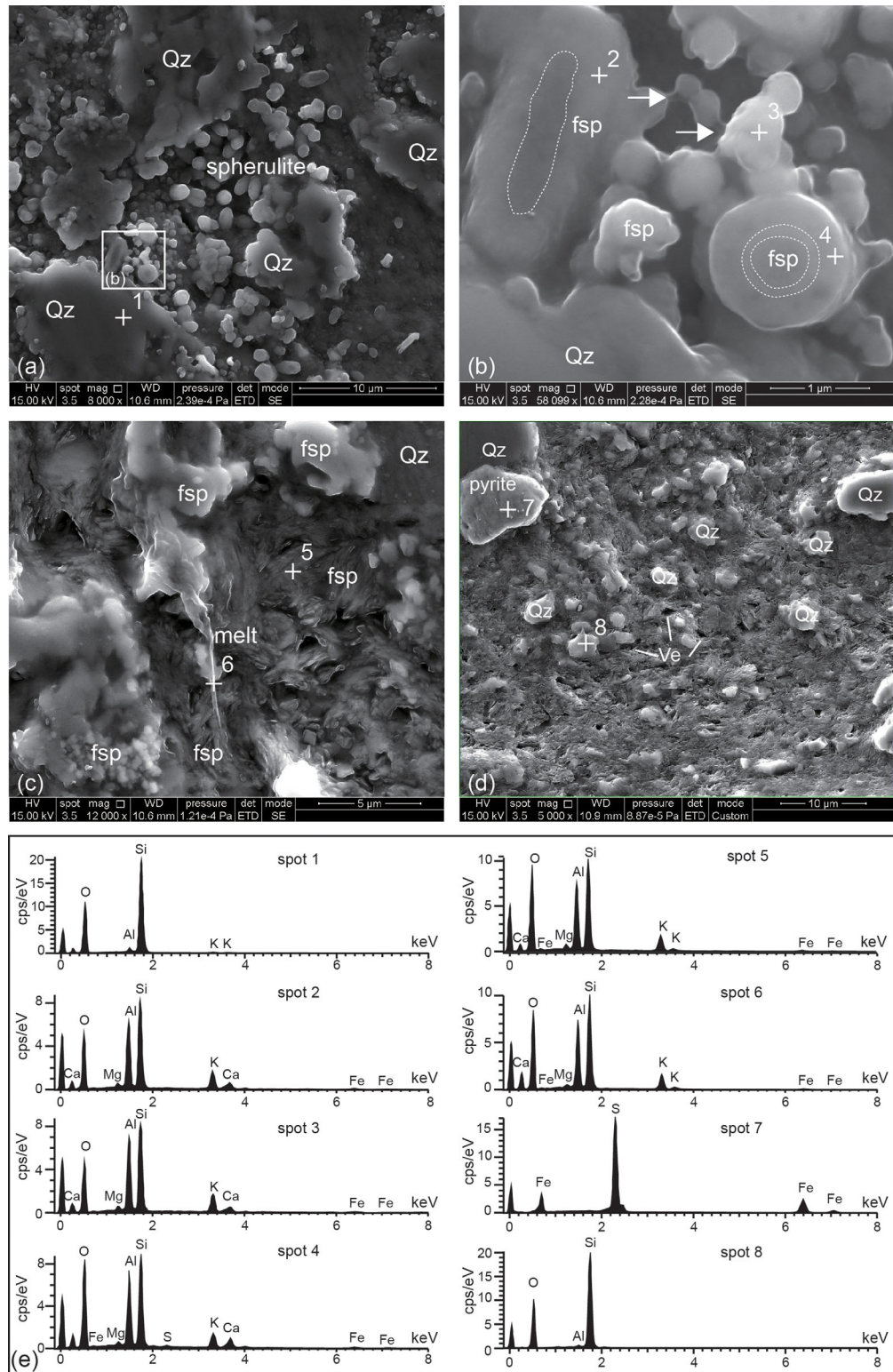


Figure 5. SEM images of the veins. (a–c) From 580.72 m-depth. (a) Melting structures of circular spherulites developed within the dark veins. (b) Expanded view of the square in Figure 5a. Note the strings of melt materials (arrows) in the gap between the spherulites and the zoning structures in circular spherulites. Quartz grain showing an embayed structure. (c) Strings of melt materials between the feldspar grain and the matrix. (d) 597.49 m-depth: vesicles of about 1 μm diameter are well-developed and well-rounded quartz grains adhere to the matrix. (e) SEM-EDX results for the spots in Figures 6b–6d (indicated by white crosses). Both structures indicate that the materials were partially melted. Qz: quartz, fsp: feldspar, Ve: vesicle.

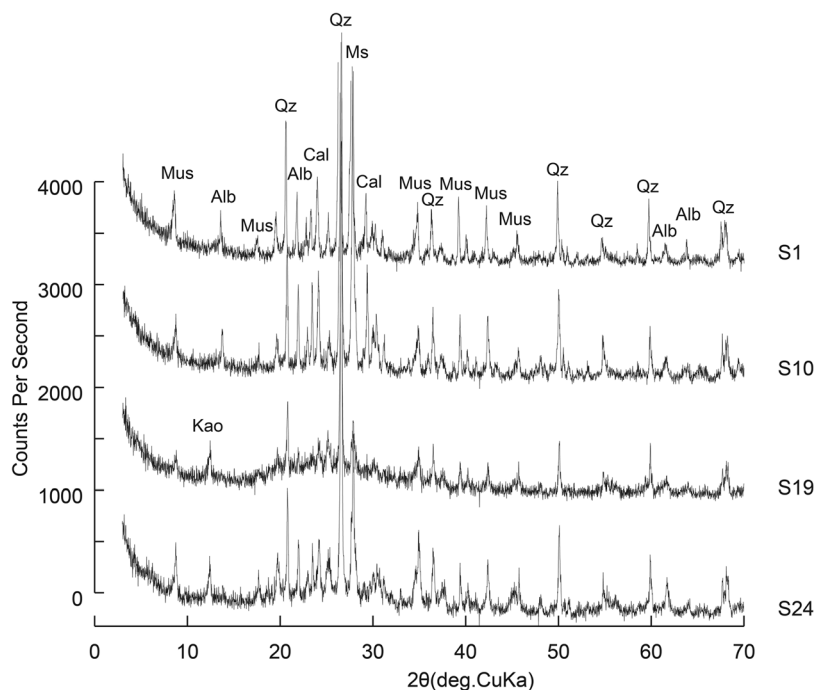


Figure 6. XRD profiles of the representative samples. S1: granodiorite; S10: cataclasite; S19: dark vein; S24: dark vein; Qz: quartz; Mus: muscovite; Cal: calcite; Alb: albite; Kao: kaolinite.

is no broad band in the range of low 2θ values in granodiorite (S1) and cataclasite (S10) (Figure 6). The spectra for S19 comprise a characteristic broad band ranging from 2θ values of 12° to 42° (Figure 6), similar to the glass pseudotachylyte veins in the Funyun fault [Lin, 1994]. The spectra for S24 also comprise an inconspicuous broad band in the range of low 2θ values (Figure 6). This indicates that the amount of remnant noncrystalline material or glass is greatest in sample S19. The presence of glass indicates that the veins have been melted. The crystal peaks in the powder X-ray diffraction patterns of S24 may indicate the partial devitrification of glassy material or glass during alteration and metamorphism during the interval following the formation of the primary glass material.

5. Rock-Magnetic Measurements

5.1. Magnetic Susceptibility

Magnetic susceptibility measurements enable the identification of different Fe-bearing minerals and estimation of their concentration or total volume [Dearing, 1999]. The results of magnetic susceptibility measurements are shown in Figure 7 (supporting information data in Table B). The magnetic susceptibility values of veins are significantly higher than those of cataclasite and granodiorite, while those for cataclasite and granodiorite are similar. The range and average magnetic susceptibility values of the veins, cataclasites, and granodiorite are $12\text{--}57 \times 10^{-6}$ and 16×10^{-6} SI; $2\text{--}10 \times 10^{-6}$ and 7×10^{-6} SI; and $1\text{--}11 \times 10^{-6}$ and 6×10^{-6} SI, respectively. The prominent magnetic susceptibility anomalies correlate well with the location of veins (Figure 7); however, black veins have higher values than gray veins, and thick veins have higher values than thin veins.

Samples	Lithology	Mineralogy
S1	Granodiorite	Quartz 41%, muscovite 21%, calcite 6%, albite 32%
S10	Cataclasite	Quartz 31%, muscovite 20%, calcite 7%, albite 41%
S19	Dark vein	Quartz 30%, muscovite 41%, kaolinite 12%, albite 17%
S24	Dark vein	Quartz 35%, muscovite 32%, kaolinite 9%, albite 24%

5.2. Magnetic Hysteresis Loops

The results of magnetic hysteresis loop measurements are shown in Figure 8 (supporting information data in Table C). The magnetic hysteresis loops of granodiorite and cataclasite before paramagnetic correction are linear, indicating that

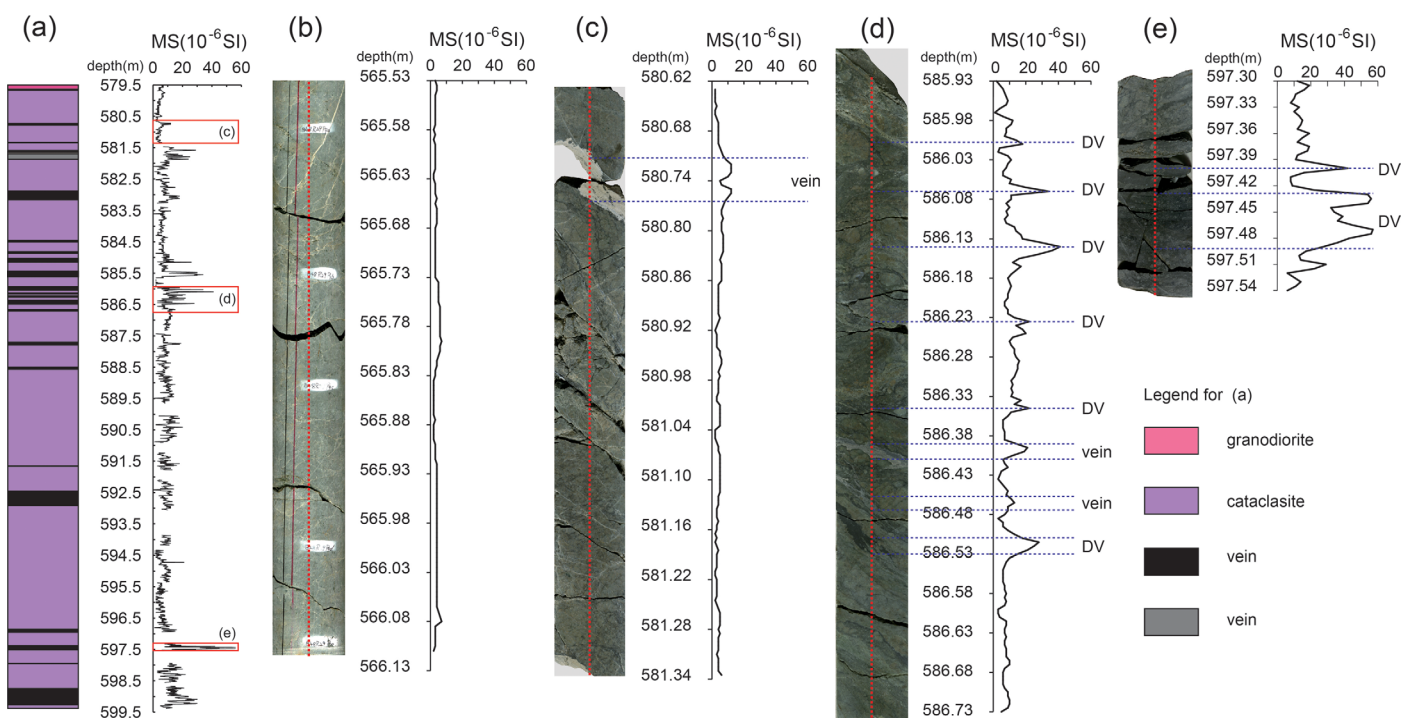


Figure 7. Magnetic susceptibility (MS) values of cores from the WFSD-2 borehole. (a) MS values of cores from 579.50 to 599.31 m-depth. (b) MS values of cores from 565.53 to 566.13 m-depth. (c–e) Enlarged areas noted in Figure 7a. MS values were measured along the red lines in the middle of cores. The peaks in MS values are often well correlated with the veins. DV: dark vein.

paramagnetic components are dominant (Figures 8a and 8c). The small goose-neck magnetic hysteresis loops below 0.1 T indicate that the granodiorite and cataclasite have a low ferromagnetic content (Figures 8a and 8c). The loops for the veins are also dominated by paramagnetic behavior (Figures 8b and 8d) but indicate that ferromagnetic material is also present. The loops for S1, S11, and S17 after para-diamagnetic correction show that these samples are saturated below 0.2 T (Figures 8a–8c), indicating the absence of high-coercivity minerals such as goethite and hematite in the gray vein and wall rocks [Roberts *et al.*, 1995; Tauxe *et al.*, 1996; Humbert *et al.*, 2012]. The loop for the dark vein (Figure 8d) after slope correction is almost saturated below 0.2 T and approximately open in high magnetic fields. The values of H_C , M_s , and M_{rs} for cataclasite are lower than those for the veins (Figure 8).

5.3. Low-Temperature Magnetic Properties

The low-temperature magnetic properties (ZFC and FC curves) of representative samples are presented in Figure 9 (supporting information Table D). Magnetite undergoes a crystallographic phase transition at around 120 K, known as the Verwey transition, which can be clearly differentiated from the transitions for hematite (263 K) and pyrrhotite (32 K) [Verwey *et al.*, 1947; Özdemir and Dunlop, 2010]. The curves for S1 and S10 reveal a Verwey transition around 120 K, indicating the presence of magnetite in granodiorite and cataclasite (Figures 9a and 9b). No transitions for hematite (263 K) or pyrrhotite (32 K) in cataclasite and granodiorite are evident in any of the curves. The remanence values in a 2.0 T field at 20 K (M_{FC}) for S1 and S10 are 36.91×10^{-5} and 24.96×10^{-5} A m² kg⁻¹, respectively; and the equivalent values in a zero field at 20 K (M_{ZFC}) are 29.79×10^{-5} and 21.98×10^{-5} A m² kg⁻¹, respectively. Similar to the wall rocks, the curves of FC and ZFC for samples S19 and S26 also indicate the occurrence of magnetite in the dark veins (Figures 9c and 9d). The remanence values in a 2.0 T field at 20 K (M_{FC}) for S19 and S26 are 50.53×10^{-5} and 44.12×10^{-5} A m² kg⁻¹, respectively; and the equivalent values in a zero field at 20 K (M_{ZFC}) are 40.90×10^{-5} and 40.65×10^{-5} A m² kg⁻¹, respectively. The remanence of dark veins is higher than that of granodiorite and cataclasite.

5.4. Thermal Demagnetization of Three-Component IRM

The thermal demagnetization of three-component IRMs have been used to identify different magnetic minerals [Lowrie, 1990; Inoue *et al.*, 2004]. The results of thermal demagnetization of three-component IRMs of

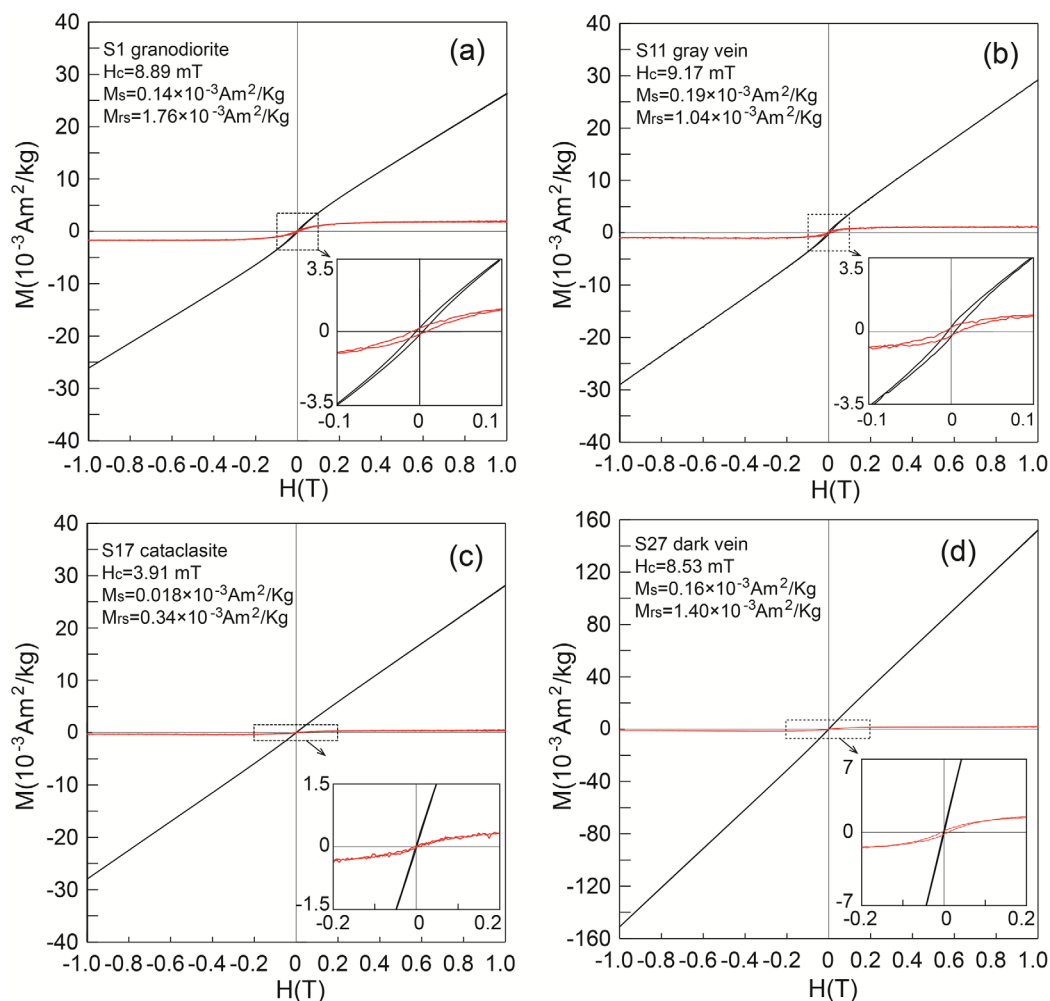


Figure 8. Magnetic hysteresis loops for representative samples before (black) and after (red) para-diamagnetic correction. The black magnetic hysteresis loops are linear with small goose-neck loops below 0.1 T.

representative samples are shown in Figure 10 (supporting information data in Table E). The curves for granodiorite and cataclasite show that the medium components are unblocked at 580°C, indicative of magnetite (Figures 10a, 10b, 10e, 10f, and 10h). However, the curves show no clear indication of goethite (80–120°C) and hematite (680°C) in granodiorite and cataclasite. The thermal demagnetization characteristics of pseudotachylyte veins resemble those of granodiorite and cataclasite (Figures 10c, 10d, 10g, and 10i). This finding implies the presence of magnetite and absence of hard minerals such as hematite and goethite in the granodiorite, cataclasite, and pseudotachylyte veins with mixed cataclasite. Decrease of the soft coercivity components at about 300–400°C was observed in some dark veins (Figures 10c and 10d). This behavior may suggest the presence of pyrrhotite or fine magnetite [Lowrie, 1990; Dunlop and Özdemir, 2000].

6. Discussion

6.1. Rock Records of Ancient Large Earthquakes Along the Longmen Shan Thrust Belt

Melt-origin pseudotachylytes are typically characterized by melt textures. They include flow structures, amygdules, microlites, spherulites, vesicles, blebs, and embayed and rounded clasts, and these features are absent in crush-origin pseudotachylytes which also contain amorphous material [Sibson, 1975; Maddock et al., 1987; Lin, 1994, 2008; Camacho et al., 1995; Lin et al., 1999, 2001; Di Toro and Pennacchioni, 2004; Ujiie et al., 2007; Otsuki et al., 2009; Janssen et al., 2010; Chu et al., 2012; Pittarello et al., 2012; Hirono et al., 2014]. Microstructural analyses, including flow structures, microlites, embayed quartz clasts, rounded quartz and

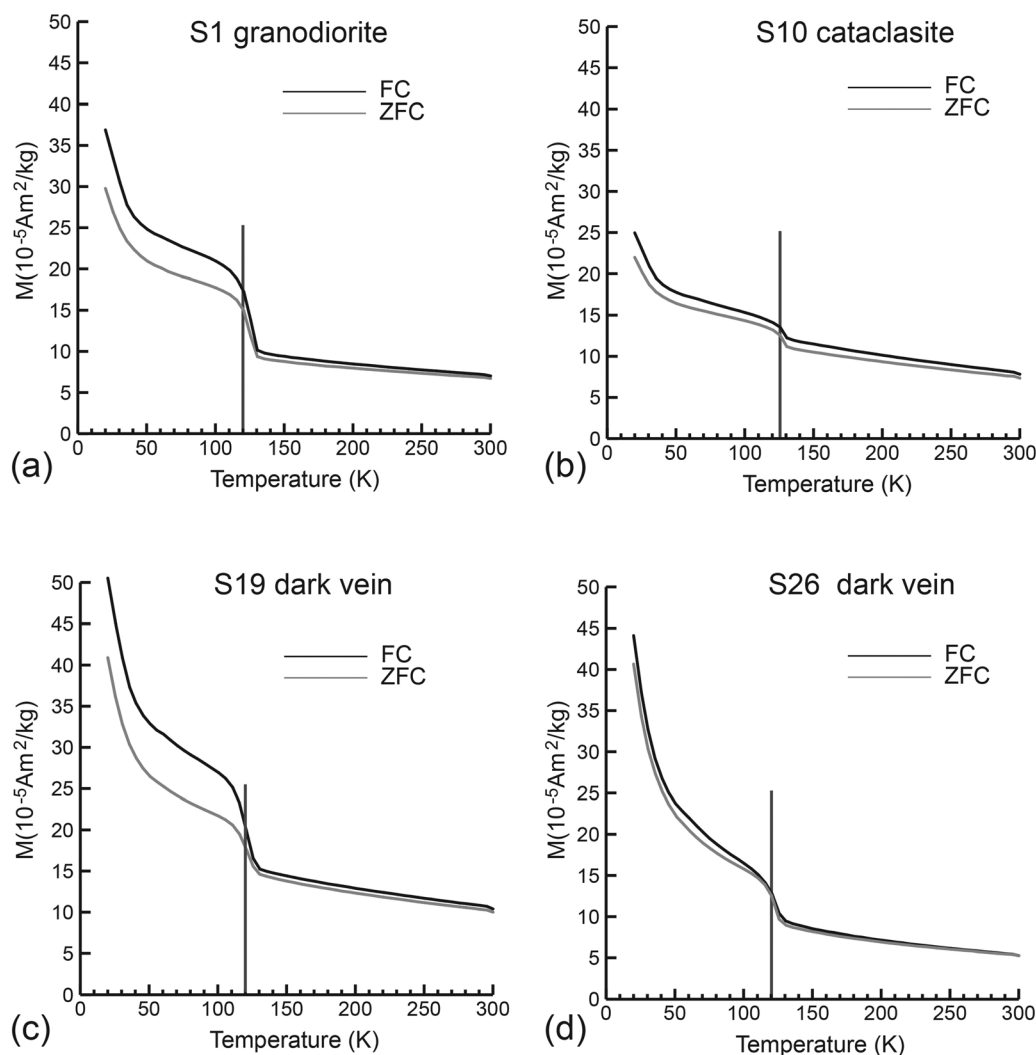


Figure 9. Results of low-temperature magnetic measurements of representative samples. The gray and black lines are the curves for ZFC and FC, respectively. All curves for ZFC and FC from representative samples exhibit a Verwey transition around 120 K, indicating the presence of magnetite. No transitions for hematite (263 K) or pyrrhotite (32 K) are evident. The remanence of the dark veins is higher than that of granodiorite and cataclasite.

feldspar grains, spherulites, vesicles, and melt flow textures within quartz grains observed in the veins, demonstrate that these veins from the WFS-2 cores are of pseudotachylytes (Figures 4 and 5). The powder X-ray diffraction spectra exhibit similar diffraction characteristics to the Fuyun glass pseudotachylyte vein, which indicates that glass is present in pseudotachylyte veins (Figure 6). The presence of glass and microstructural analyses indicates that the pseudotachylytes are of melt-origin. Previous studies concluded that ultrafine spherulites are the result of frictional melting [Lin, 1994; Kuo *et al.*, 2015]. In this study, the ultrafine spherulites in the pseudotachylyte vein imply that the seismic fault slip experienced temperatures above 1100°C (corresponding to the breakdown temperature of feldspar) [Spray, 1992]. In addition, the deep embayed quartz clasts, rounded quartz grains, and flow textures in quartz indicate that temperatures attained at least 1730°C (at least locally), as reported in the pseudotachylyte veins in the YBF zone [Wang *et al.*, 2015]. The breakdown temperature of quartz is 1730°C [Spray, 1992].

Previous studies imply that an individual pseudotachylyte vein can show evidence of an individual slip event [Di Toro and Pennacchioni, 2005; Griffith *et al.*, 2008; Alder *et al.*, 2016]. Shigetomi and Lin [1999] suggested that a single seismic faulting event cannot generate distinct multilayers with sharp boundaries. Mitchell *et al.* [2016] reported that pseudotachylytes weld the seismic fault, resulting in subsequent seismic ruptures preferably branching onto other fractures or foliation planes. Based on macroscopic and

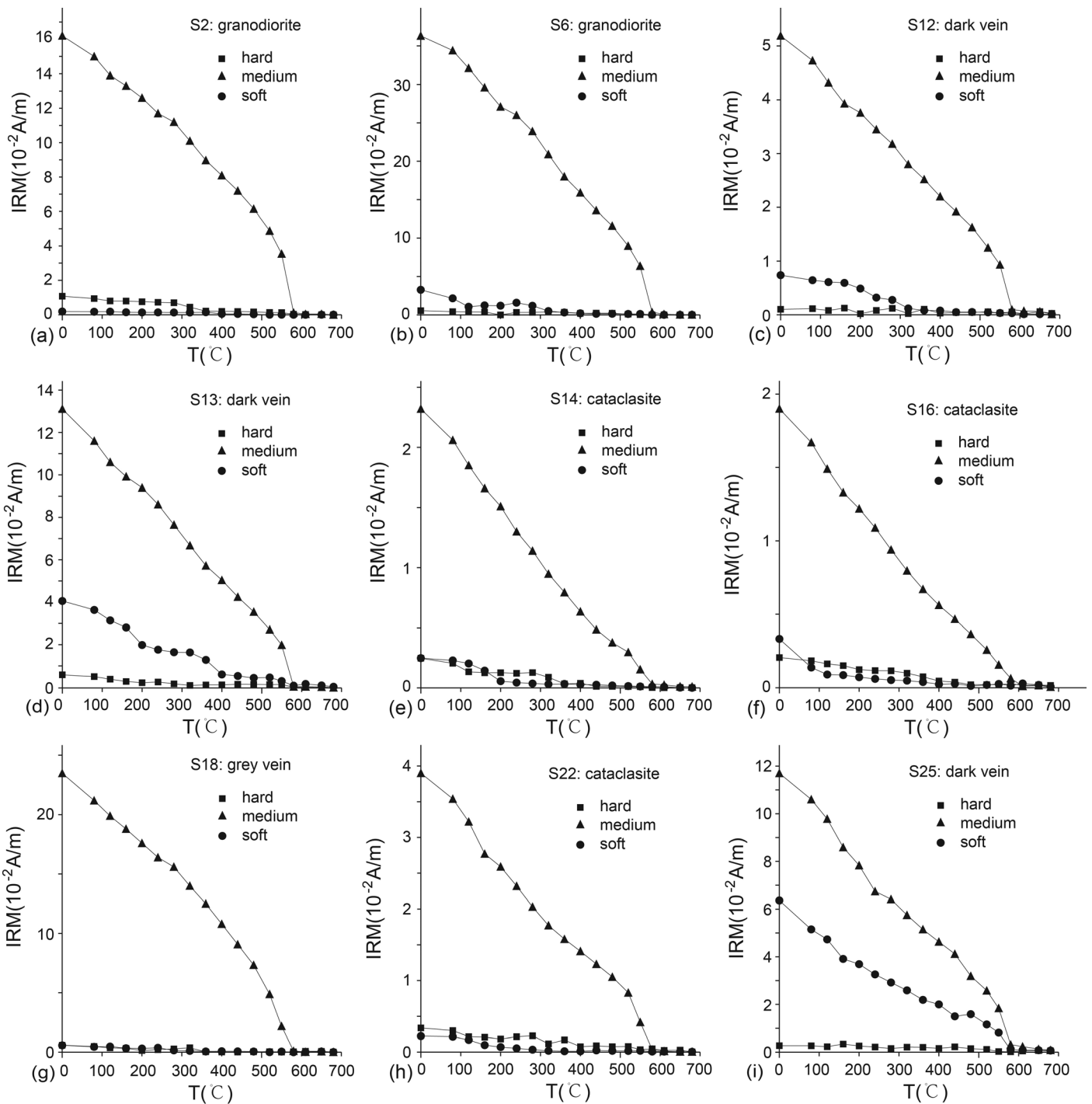


Figure 10. Results of three-axis thermal demagnetization of IRMs for representative samples. The unblocking temperatures are around 580°C, and there is no clear indication of goethite (80–120°C), pyrrhotite (300–330°C), or hematite (680°C) in any of the samples.

microstructural analyses, different pseudotachylyte layers were present in the WFSD-2 cores (Figures 2–4). If each pseudotachylyte layer records at least one earthquake, 21 generations of pseudotachylytes can be determined based on the various locations (supporting information Figure A). The gray veins may indicate the partial devitrification of glassy material or glass during alteration and metamorphism during the interval following the formation of the dark pseudotachylyte veins. The gray veins (Figures 3a–3c) and dark veins may imply different stages of pseudotachylytes. In the cores, fragments of black pseudotachylyte are

identified in the gray vein (Figure 3a), and in addition, parallel black veins, gray veins, and dark-gray veins with sharp boundaries are observed (Figures 3c and 3d). The black pseudotachylyte veins injected and wedged out into the gray vein suggest that gray veins are formed earlier than black veins. In optical microscopy, fragments of black pseudotachylyte are recognized in dark-gray pseudotachylyte (Figure 4b). In addition, the dark vein cuts off one clast from another dark vein (Figure 4c). The fragments of early-formed pseudotachylyte in the new layer suggest that subsequent seismic ruptures occurred on the same fracture. The occurrence of seismic faulting processes exploiting the same fault strand twice may be inconsistent with the results of Mitchell *et al.* [2016]. Overprinting relations between different layers of pseudotachylyte veins are visible in microstructural observations (Figures 4b–4d). These structures imply that the pseudotachylyte veins in the WFSD-2 cores are the products of multiple seismic faulting events, and therefore, ancient earthquakes may have occurred repeatedly within the Longmen Shan thrust belt. This conclusion is in accord with that based on studies of fault rocks, microstructural analyses, and magnetic properties of outcrops of the study area [Zhang *et al.*, 2012; Li *et al.*, 2013; Pei *et al.*, 2014a, 2016; Wang *et al.*, 2014, 2015].

6.2. Rock-Magnetic Response to Large Earthquakes

Previous rock-magnetic studies have indicated that pseudotachylytes have relatively high magnetic susceptibility values, and it has been suggested that they may result from (1) ferromagnetic grains being crushed to submicrometer size [Dearing, 1999] and/or (2) ferromagnetic minerals being newly formed by thermal decomposition of paramagnetic components during a large earthquake [Fukuchi, 2003; Fukuchi *et al.*, 2005; Mishima *et al.*, 2006; Hirono *et al.*, 2006b; Ferré *et al.*, 2005, 2012]. Therefore, a positive magnetic susceptibility anomaly can be regarded as evidence for large earthquakes. In this study, magnetic susceptibility anomalies are also evident in pseudotachylyte veins (Figure 7), the values being 2–10 times higher than in cataclasites. In addition, the large number of magnetic susceptibility anomalies in the cataclasite zone suggest repeated earthquake faulting (Figure 7a).

In general, it is difficult to identify magnetic minerals using optical or electron microscopy alone because of their low concentration and small grain size in pseudotachylytes. However, the type, size, and concentration of magnetic minerals can be determined more easily using rock-magnetic methods [Hunt *et al.*, 1995; Dunlop and Özdemir, 1997; Deng *et al.*, 2001; Liu *et al.*, 2005]. The magnetic hysteresis loops indicate that the magnetic behavior of the cataclasites and wall rocks are controlled by paramagnetic minerals (Figure 8). Previous rock-magnetic studies in the Yingxiu-Beichuan fault zone also suggest that the magnetic behavior of fault rocks and wall rocks is controlled by paramagnetic minerals [Pei *et al.*, 2014a; Liu *et al.*, 2016; Yang *et al.*, 2016]. In addition, the small goose-neck magnetic hysteresis loops below 0.1 T indicate very low concentrations of ferromagnetic minerals in the samples (Figure 8). The magnetic hysteresis loop of the dark vein after slope correction is saturated around 0.2 T but is approximately open in higher magnetic fields (Figure 8d). To identify the magnetic minerals, the measurements of the low-temperature magnetic properties and the thermal demagnetization of three-component IRM were carried out for the representative samples. Low-temperature magnetic measurements (FC and ZFC curves) reveal a Verwey transition around 120 K, implying the presence of magnetite (Figures 9b and 9d). No transitions for hematite (263 K) or pyrrhotite (32 K) are evident in the FC and ZFC curves of pseudotachylyte veins. This finding suggests that the low unblocking spectrum of “soft” component at 300–400°C observed in some dark veins (Figures 10c and 10d) could be the consequence of fine magnetite. The thermal demagnetization of three-component IRM for all samples indicates the presence of magnetite and the absence of goethite and hematite (Figure 10). Therefore, the ferromagnetic mineralogy is dominated by magnetite grains with different sizes in pseudotachylyte veins. The heating curves of the pseudotachylyte decrease to near zero around 580°C (Figures Be and Bf in the supporting information), also implying the presence of magnetite. Similarly, these findings including magnetic hysteresis loops, low-temperature magnetic measurements, and the thermal demagnetization of three-component IRM demonstrate that the magnetic minerals in granodiorite and cataclasite are paramagnetic minerals with relatively small amounts of magnetite.

It has been suggested that a reduction in the size of ferromagnetic grains from submicron to superparamagnetic results is responsible for the high magnetic susceptibility values of fault rocks [Dearing, 1999; Hirono *et al.*, 2006b]. The higher M_r/M_s ratios of the samples from the pseudotachylyte veins, cataclasites, and granodiorite indicate a range of magnetic domain states from MD to PSD (Figure 8). Consequently, the inferred grain sizes are too large to produce a significant increase in the magnetic susceptibility [Dunlop, 2002;

Mishima et al., 2009], and therefore a reduction in the grain size of the ferromagnetic minerals is not a plausible explanation for the high magnetic susceptibility values of the pseudotachylyte.

The ZFC, FC curves, and results of thermal demagnetization of three-component IRM imply that the main ferromagnetic mineral in pseudotachylyte veins and wall rocks is magnetite. In addition, the higher saturation magnetization (M_s) in pseudotachylyte veins than in granodiorite and cataclasite indicates that more magnetite is present in pseudotachylyte veins than in wall rocks (Figure 8). H_c and M_{rs} are also higher in pseudotachylyte veins than in wall rocks, while the increases in remanence at 20 K (Figure 9) in pseudotachylyte veins also suggest a higher ferromagnetic mineral content. Magnetite can be formed by the breakdown of ferromagnesian silicates and liberation of Fe at elevated temperatures from frictional melts in pseudotachylytes [*Nakamura et al.*, 2002; *Ferré et al.*, 2005, 2012]. Decomposition of siderite and chlorite to magnetite was caused by frictional heating in the Chelungpu fault [*Tanikawa et al.*, 2008]. SD to PSD magnetite was formed by oxidation of Fe from the breakdown of ferromagnesian silicate during melting in experimental pseudotachylytes [*Nakamura et al.*, 2002]. A previous rock-magnetic study indicated that paramagnetic minerals (such as siderite and lepidocrocite) and pyrrhotite may have been transformed to magnetite/maghemite in the Longmen Shan thrust belt [*Yang et al.*, 2012a]. Fault-rock-magnetic measurements of the Zhaojiagou outcrop indicate that some Fe-bearing minerals (lepidocrocite, smectite, siderite, and chlorite) can be transformed to magnetite/maghemite [*Yang et al.*, 2012b]. *Pei et al.* [2014a] and *Liu et al.* [2016] reported that magnetite was newly formed by the breakdown of paramagnetic minerals at the Bajiamiao outcrop in the Yingxiu-Beichuan fault. In our study, the pseudotachylyte veins, granodiorite, and cataclasite are characterized by an abundance of paramagnetic minerals and small amounts of magnetite. Magnetite is enriched in the pseudotachylyte veins, which have higher magnetic susceptibility values than granodiorite and cataclasite. We conclude that in the WFSD-2 cores, the neoformation of magnetite from the breakdown of Fe-bearing paramagnetic minerals by frictional heating is responsible for the higher magnetic susceptibility values in the pseudotachylyte veins.

Numerous rock-magnetic studies of fault rocks have focused on characterizing magnetic changes resulting from thermal decomposition due to seismic frictional heating [*Mishima et al.*, 2006; *Hirono et al.*, 2006a; *Tanikawa et al.*, 2008; *Pei et al.*, 2014a,b]. *Yang et al.* [2016] studied rock-fluid interactions in fault zones and emphasized the role of fluid in the transformation of magnetic minerals within fault gouge. Generally, cataclasite is formed at depths of 10–15 km, while the fault gouge and fault breccia are formed at shallower depths of <5 km [*Sibson*, 1977]. Fluid infiltration within fault breccia and gouge is stronger than in the cataclasite zone. The presence of calcite in the cataclasite zone (Table 2 and Figure 3e) implies the presence of seismic hot fluids in the cataclasite zone within the WFSD-2 cores. However, experiments performed at a low confining pressure indicated that the highest permeabilities occur in the damaged zone [*Evans et al.*, 1997]. Pseudotachylyte veins are stiffer and more cohesive than cataclasites. The abundance of calcite in the cataclasites (Table 2) also indicates that cataclasites are the main channel for fluids. However, the cataclasites have not experienced seismic frictional heating, and therefore in the absence of frictional heating, fluid infiltration played a minor role in the growth of magnetic minerals within fault zones. Therefore, seismic frictional heating may be mainly responsible for the magnetic properties of pseudotachylyte veins. *Zhang et al.* [2017] also suggested that the transformation of magnetic minerals in pseudotachylytes is mainly caused by frictional heating during large earthquakes.

The presence of new-formed magnetic minerals is also an indicator of a certain degree of temperature elevation [*Chou et al.*, 2012b]. *Pan et al.* [2000] reported that siderite could be transformed to ferromagnetic phases at temperatures of 400–530°C, into magnetite at temperatures of 540–590°C, and into hematite at a temperature of 700°C. *Liu and Deng* [2009] reported that the neoformation of SD magnetite begins to occur above 400°C, and most of the neoformed fine-grained (SP + SD) particles with a dominant grain size around 35 nm are produced above 500°C. Rock-magnetic studies indicate that siderite and pyrite were transformed into magnetite and pyrrhotite at >400°C–500°C during the Taiwan Chi-Chi earthquake [*Tanikawa et al.*, 2008; *Chou et al.*, 2012b]. Previous rock-magnetic studies of gouge in the Yingxiu-Beichuan fault zone indicated that pyrrhotite formed at temperatures >500°C [*Liu et al.*, 2016]. Parts of the magnetite grains in pseudotachylytes from the WFSD-2 cores are inherited from the host rock, while most of the magnetite is newly formed by frictional heating during large earthquakes. The application of previous findings to our own study leads us to infer that the new-formed magnetite from the Fe-bearing paramagnetic minerals indicates that the pseudotachylytes have experienced temperatures of >500°C. Overall, the rock-magnetic results

indicate that the fault zone has experienced temperatures exceeding 500°C. These temperatures are the result of frictional heating produced by large earthquakes.

In Longmen Shan thrust belt, ancient large earthquakes occurred repeatedly from around 3000–6000 years ago at 10–14 km-depth [Li *et al.*, 2008; Zhang *et al.*, 2008; Zheng *et al.*, 2016]. These seismic faulting events experienced high temperatures (>500°C) which caused the physical and chemical alteration of the magnetic mineral assemblages within the host rocks. Magnetite may be formed by the thermal decomposition of paramagnetic phases due to frictional heating during large earthquakes. The new-formed magnetite is responsible for the high magnetic susceptibility anomalies in pseudotachylyte veins in the WFSD-2 cores. Numerous high magnetic susceptibility anomalies and layers of pseudotachylyte veins within the WFSD-2 cores demonstrate that powerful seismic faulting events occurred repeatedly in the Longmen Shan thrust belt.

7. Conclusions

The 19.69 m-thick cataclasite zone in the WFSD-2 borehole cores is a product of repeated earthquakes. Detailed rock-magnetic, microstructural, mineralogical, and chemical analyses were conducted on the pseudotachylyte veins and wall rock (granodiorite and cataclasite). The results reveal distinctive microstructural structures, geochemical compositions, and magnetic properties in granodiorite, cataclasites, and pseudotachylyte veins. The main conclusions are summarized as follows.

1. XRD spectra indicate that glass is present in the veins. This finding, together with the presence of flow structures, microlites, embayed quartz clasts, rounded quartz and feldspar grains, spherulites, vesicles, and melt flow textures in quartz, indicates that the veins in the WFSD-2 cores are melt-origin pseudotachylytes.
2. Twenty-one layers of pseudotachylytes observed in WFSD-2 cores demonstrate that at least 21 powerful seismic faulting events occurred repeatedly in the Longmen Shan thrust belt. The fragments of early-formed pseudotachylytes in the new layer suggest that subsequent seismic ruptures occurred on the same fracture.
3. Pseudotachylyte veins have higher magnetic susceptibility values than cataclasite and granodiorite. Neoformed magnetite from the thermal decomposition of paramagnetic minerals contributes to the higher magnetic susceptibility values in the pseudotachylyte veins.
4. Magnetic analyses indicate that frictional heating (>500°C) has occurred in the Longmen Shan thrust belt during the slip of repeated large earthquakes. The seismic frictional heating may play the dominant role in generating the magnetic properties of pseudotachylyte veins.

Acknowledgments

This work is supported by the National Natural Science Foundation of China (grants 41520104006, 41330211, 41672218, 41473006, and 41673011), and the Special Funds of Basic Scientific Research Expenses of CAGS (grants YYWF201601 and YYWF201613). We are grateful to the working group of the Wenchuan Earthquake Fault Scientific Drilling. We thank L. W. Kuo of Taiwan Central University, Taipei, for constructive discussions; Y. Zhao, M. K. Bai, C. L. Ge, S. Han, J. C. Wei, and J. G. Wu, for helping to prepare samples; C. F. Zhou and S. C. Liu of the State Key Laboratory of Lithospheric Evolution, Institute of Geology and Geophysics, Chinese Academy of Sciences, Beijing, for help with rock-magnetic measurements; and Y. J. Lin of Taiwan University, Taipei, for help with SEM analyses. We want to thank Eric Ferré, anonymous reviewer, and Associate Editor Joshua Feinberg for useful suggestions which significantly improved the manuscript. Data supporting this study are available in supporting information Figures A and B and supporting information Tables A–E.

References

- Alder, S., S. A. F. Smith, and J. M. Scott (2016), Fault-zone structure and weakening processes in basin-scale reverse faults: The Moonlight Fault Zone, South Island, New Zealand, *J. Struct. Geol.*, *91*, 177–194, doi:10.1016/j.jsg.2016.09.001.
- Andersen, T. B., and H. Austrheim (2006), Fossil earthquakes recorded by pseudotachylytes in mantle peridotite from the Alpine subduction complex of Corsica, *Earth Planet. Sci. Lett.*, *242*, 58–72, doi:10.1016/j.epsl.2005.11.058.
- Biegel, R. L., and C. G. Sammis (2004), Relating fault mechanics to fault zone structure, *Adv. Geophys.*, *47*, 65–111.
- Camacho, A., R. H. Vernon, and J. D. Fitz Gerald (1995), Large volumes of anhydrous pseudotachylyte in the Woodroffe Thrust, eastern Musgrave Ranges, Australia, *J. Struct. Geol.*, *17*, 371–383.
- Chester, F. M., and J. S. Chester (1998), Ultracataclasite structure and friction processes of the Punchbowl fault, San Andreas system, California, *Tectonophysics*, *295*, 199–221.
- Chester, M. (1995), A rheologic model for wet crust applied to strike-slip faults, *J. Geophys. Res.*, *100*, 13,033–13,044.
- Chou, Y.-M., S.-R. Song, C. Aubourg, T. Q. Lee, A.-M. Boullier, Y.-F. Song, E.-C. Yeh, L.-W. Kuo, and C. Y. Wang (2012a), An earthquake slip zone is a magnetic recorder, *Geology*, *40*(6), 551–554.
- Chou, Y.-M., S.-R. Song, C. Aubourg, Y.-F. Song, A.-M. Boullier, T.-Q. Lee, M. Evans, E.-C. Yeh, and Y.-M. Chen (2012b), Pyrite alteration and neoformed magnetic minerals in the fault zone of the Chi-Chi earthquake (Mw 7.6, 1999): Evidence for frictional heating and co-seismic fluids, *Geochem. Geophys. Geosyst.*, *13*, Q08002, doi:10.1029/2012GC004120.
- Chu, H. T., S. L. Hwang, P. Shen, and T. F. Yui (2012), Pseudotachylyte in the Tananao Metamorphic Complex, Taiwan: Occurrence and dynamic phase changes of fossil earthquakes, *Tectonophysics*, *581*, 62–75.
- Dearing, J. (1999), Magnetic susceptibility, in *Environmental Magnetism: A Practical Guide*, edited by J. Walden, F. Oldfield, and J. Smith, pp. 35–62, Quat. Res. Assoc., London, U. K.
- Deng, C. L., R. X. Zhu, M. J. Jackson, K. L. Verosub, and M. J. Singer (2001), Variability of the temperature-dependent susceptibility of the Holocene eolian deposits in the Chinese loess plateau: A pedogenesis indicator, *Phys. Chem. Earth A*, *26*, 873–878.
- Densmore, A. L., M. A. Ellis, Y. Li, R. J. Zhou, G. S. Hancock, and N. Richardson (2007), Active tectonics of the Beichuan and Pengguan faults at the eastern margin of the Tibetan Plateau, *Tectonics*, *26*, TC4005, doi:10.1029/2006TC001987.

- Di Toro, G., and G. Pennacchioni (2004), Superheated friction-induced melts in zoned pseudotachylites within the Adamello tonalites (Italian Southern Alps), *J. Struct. Geol.*, *26*, 1783–1801, doi:10.1016/j.jsg.2004.03.001.
- Di Toro, G., and G. Pennacchioni (2005), Fault plane processes and mesoscopic structure of a strong type seismogenic fault in tonalites (Adamello batholith, Southern Alps), *Tectonophysics*, *402*, 55–80, doi:10.1016/j.tecto.2004.12.036.
- Dunlop, D. J. (2002), Theory and application of the Day plot (*Mrs/Ms* versus *Hcr/Hc*) 2. Application to data for rocks, sediments, and soils, *J. Geophys. Res.*, *107*(B3), doi:10.1029/2001JB000487.
- Dunlop, D. J., and Ö. Özdemir (1997), *Rock Magnetism: Fundamentals and Frontiers*, Cambridge Univ. Press, Cambridge, U. K.
- Dunlop, D. J., and Ö. Özdemir (2000), Effect of grain size and domain state on thermal demagnetization tails, *Geophys. Res. Lett.*, *27*, 1311–1314, doi:10.1029/1999GL008461.
- Evans, J. P., C. B. Forster, and J. V. Goddard (1997), Permeability of fault-related Rocks, and implications for hydraulic structure of fault zones, *J. Struct. Geol.*, *19*(11), 1393–1404.
- Faulkner, D. R., T. M. Mitchell, E. H. Rutter, and J. Cembrano (2008), On the structure and mechanical properties of large strike-slip faults, *Geol. Soc. Spec. Publ.*, *299*, 139–150.
- Ferré, E. C., M. S. Zechmeister, J. W. Geissman, N. MathanaSekaran, and K. Kocak (2005), The origin of high magnetic remanence in fault pseudotachylites: Theoretical considerations and implication for coseismic electrical currents, *Tectonophysics*, *402*(1–4), 125–139.
- Ferré, E. C., J. W. Geissman, and M. S. Zechmeister (2012), Magnetic properties of fault pseudotachylites in granites, *J. Geophys. Res.*, *117*, B01106, doi:10.1029/2011JB008762.
- Fukuchi, T. (2003), Strong ferrimagnetic resonance signal and magnetic susceptibility of the Nojima pseudotachylite in Japan and their implication for coseismic electromagnetic changes, *J. Geophys. Res.*, *108*(B6), 2312, doi:10.1029/2002JB002007.
- Fukuchi, T., K. Mizoguchi, and T. Shimamoto (2005), Ferrimagnetic resonance signal produced by frictional heating: A new indicator of paleoseismicity, *J. Geophys. Res.*, *110*, B12404, doi:10.1029/2004JB003485.
- Griffith, W. A., G. Di Toro, G. Pennacchioni, and D. D. Pollard (2008), Thin pseudotachylites in faults of the Mt. Abbot quadrangle, Sierra Nevada: Physical constraints for small seismic slip events, *J. Struct. Geol.*, *30*, 1086–1094, doi:10.1016/j.jsg.2008.05.003.
- Hirono, T., et al. (2006a), Evidence of frictional melting from disk-shaped black material, discovered within the Taiwan Chelungpu fault system, *Geophys. Res. Lett.*, *33*, L19311, doi:10.1029/2006GL027329.
- Hirono, T., et al. (2006b), High magnetic susceptibility of fault gouge within Taiwan Chelungpu fault: Nondestructive continuous measurements of physical and chemical properties in fault rocks recovered from Hole B, TCDP, *Geophys. Res. Lett.*, *33*, L15303, doi:10.1029/2006GL026133.
- Hirono, T., J. Kameda, H. Kanda, W. Tanikawa, and T. Ishikawa (2014), Mineral assemblage anomalies in the slip zone of the 1999 Taiwan Chi-Chi earthquake: Ultrafine particles preserved only in the latest slip zone, *Geophys. Res. Lett.*, *41*, 3052–3059, doi:10.1002/2014GL059805.
- Humbert, F., P. Robion, L. Louis, D. L. Bartier, B. A. Ledésert, and S.-R. Song (2012), Magnetic inference of in situ open microcracks in sandstone samples from the Taiwan Chelungpu Fault Drilling Project (TCDP), *J. Asian Earth Sci.*, *45*, 179–189, doi:10.1016/j.jseae.2011.10.009.
- Hunt, C. P., S. K. Banerjee, J. Han, P. A. Solheld, E. Oches, W.-W. Sun, and T. Liu (1995), Rock-magnetic proxies of climate change in the loess-palaeosol sequences of the western Loess Plateau of China, *Geophys. J. Int.*, *123*, 232–244, doi:10.1111/j.1365-246X.1995.tb06672.x.
- Inoue, S., A. Hayashida, M. Katoc, H. Fukusawac, and Y. Yasuda (2004), Environmental magnetism of brackish-water sediments from Lake Tougou-ike on the Japan Sea coast, *Quat. Int.*, *123–125*, 35–41, doi:10.1016/j.quaint.2004.02.006.
- Janssen, C., R. Wirth, E. Rybacki, R. Naumann, H. Kemnitz, H. R. Wenk, and G. Dresen (2010), Amorphous material in SAFOD core samples (San Andreas Fault): Evidence for crush-origin pseudotachylites?, *Geophys. Res. Lett.*, *37*, L01303, doi:10.1029/2009GL040993.
- Kuo, L.-W., H. B. Li, S. A. F. Smith, G. Di Toro, J. Suppe, S.-R. Song, S. Nielsen, H.-S. Sheu, and J. L. Si (2014), Gouge graphitization and dynamic fault weakening during the 2008 Mw 7.9 Wenchuan earthquake, *Geology*, *42*(1), 47–50.
- Kuo, L.-W., Y.-F. Song, C.-M. Yang, S.-R. Song, C.-C. Wang, J.-J. Dong, J. Suppe, and T. Shimamoto (2015), Ultrafine spherical quartz formation during seismic fault slip: Natural and experimental evidence and its implications, *Tectonophysics*, *664*, 98–108.
- Li, H. B., Z. X. Wang, X. F. Fu, L. W. Hou, J. L. Si, Z. L. Qiu, N. Li, and F. R. Fu (2008), The surface rupture zone distribution of the Wenchuan earthquake (Ms 8.0) happened on May 12th, 2008 [in Chinese], *Geol. China*, *35*(5), 803–813.
- Li, H. B., et al. (2013), Characteristics of the fault-related rocks, fault zones and the principal slip zone in the Wenchuan Earthquake Fault Scientific Drilling Project Hole-1 (WFSD-1), *Tectonophysics*, *584*, 23–42.
- Li, H. B., et al. (2014), Structural and physical property characterization in the Wenchuan Earthquake Fault Scientific Drilling project – hole 1 (WFSD-1), *Tectonophysics*, *619–620*, 86–100.
- Li, H. B., et al. (2016), Lithological and structural characterization of the Longmen Shan fault belt from the 3rd hole of the Wenchuan Earthquake Fault Scientific Drilling project (WFSD-3), *Int. J. Earth Sci.*, *105*(8), 2253–2272, doi:10.1007/s00531-015-1285-9.
- Li, Y., R. J. Zhou, A. L. Densmore, M. A. Ellis, and B. Li (2006), Sedimentary responses to Late Cenozoic thrusting and strike-slipping of Longmen Shan along eastern margin of Tibetan Plateau [in Chinese], *Acta Sediment. Sin.*, *24*(2), 153–164.
- Lin, A. M. (1994), Glassy pseudotachylite veins from the Fuyun Fault zone, Northwest China, *J. Struct. Geol.*, *16*, 71–83.
- Lin, A. M. (1999), Roundness of clasts in pseudotachylites and cataclastic rocks as an indicator of frictional melting, *J. Struct. Geol.*, *21*, 473–478.
- Lin, A. M. (2008), *Fossil Earthquakes: The Formation and Preservation of Pseudotachylites [in Chinese]*, pp. 1–321, Higher Educ. Press, Beijing.
- Lin, A. M., and T. Shimamoto (1998), Selective melting processes as inferred from experimentally generated pseudotachylites, *J. Asian Earth Sci.*, *16*(5–6), 533–545.
- Lin, A. M., A. Chen, C. F. Liau, C. T. Lee, C. C. Lin, P. S. Lin, S. C. Wen, and T. Ouchi (2001), Frictional melting due to coseismic landsliding during the 1999 Chi-Chi (Taiwan) ML 7.3 earthquake, *Geophys. Res. Lett.*, *28*, 4011–4014.
- Liu, D. L., H. B. Li, T. Q. Lee, Y.-M. Chou, S.-R. Song, Z. M. Sun, M. L. Chevalier, and J. L. Si (2014), Primary rock magnetism for the Wenchuan earthquake fault zone at Jiulong outcrop, Sichuan Province, China, *Tectonophysics*, *619–620*, 58–69.
- Liu, D. L., H. B. Li, T. Q. Lee, Z. M. Sun, J. Liu, L. Han, and M. L. Chevalier (2016), Magnetic mineral characterization close to the Yingxiu-Beichuan fault surface rupture zone of the Wenchuan earthquake (Mw 7.9, 2008) and its implication for earthquake slip processes, *J. Asian Earth Sci.*, *115*, 468–479.
- Liu, Q. S., and C. L. Deng (2009), Magnetic susceptibility and its environmental significances [in Chinese], *Chin. J. Geophys.*, *52*(4), 1041–1048, doi:10.3969/j.issn.0001-5733.2009.04.021.
- Liu, Q. S., C. L. Deng, Y. J. Yu, J. Torrent, M. J. Jackson, S. K. Banerjee, and R. X. Zhu (2005), Temperature dependence of magnetic susceptibility in an argon environment: Implications for pedogenesis of Chinese loess/palaeosols, *Geophys. J. Int.*, *161*, 102–112, doi:10.1111/j.1365-246X.2005.02564.x.
- Loubser, M., and S. Verryin (2008), Combining XRF and XRD analyses and sample preparation to solve mineralogical problems, *S. Afr. J. Geol.*, *111*, 229–238, doi:10.2113/gssajg.111.2-3.229.

- Lowrie, W. (1990), Identification of ferromagnetic minerals in a rock by coercivity and unblocking temperature properties, *Geophys. Res. Lett.*, *17*, 159–162.
- Maddock, R. H., J. Grocott, and M. Van Nes (1987), Vesicles, amygdalae and similar structures in fault-generated pseudotachylytes, *Lithos*, *20*, 419–432.
- Magloughlin, J. F. (1992), Microstructural and chemical changes associated with cataclasis and frictional melting at shallow crustal levels: The cataclase-pseudotachylyte connection, *Tectonophysics*, *204*, 243–260, doi:10.1016/0040-1951(92)90310-3.
- Mishima, T., T. Hirono, W. Soh, and S.-R. Song (2006), Thermal history estimation of the Taiwan Chelungpu fault using rock-magnetic methods, *Geophys. Res. Lett.*, *33*, L23311, doi:10.1029/2006GL028088.
- Mishima, T., T. Hirono, N. Nakamura, W. Tanikawa, W. Soh, and S.-R. Song (2009), Changes to magnetic minerals caused by frictional heating during the 1999 Taiwan Chi-Chi earthquake, *Earth Planets Space*, *61*(6), 797–801.
- Mitchell, T. M., V. Toy, G. Di Toro, J. Renner, and R. H. Sibson (2016), Fault welding by pseudotachylyte formation, *Geology*, *44*, 1059–1062, doi:10.1130/G38373.1.
- Nakamura, N., and Y. Iyeda (2005), Magnetic properties and paleointensity of pseudotachylytes from the Sudbury structure, Canada: Petrologic control, *Tectonophysics*, *402*, 141–152.
- Nakamura, N., T. Hirose, and G. J. Borradaile (2002), Laboratory verification of submicron magnetite production in pseudotachylytes: Relevance for paleointensity studies, *Earth Planet. Sci. Lett.*, *201*, 13–18.
- Otsuki, K., T. Hirono, M. Omori, M. Sagaguchi, W. Tanigawa, W. Lin, W. Soh, and S.-R. Song (2009), Analyses of pseudotachylyte from Hole-B of Taiwan Chelungpu Fault Drilling Project (TCDFP); their implications for seismic slip behaviors during the 1999 Chi-Chi earthquake, *Tectonophysics*, *469*, 13–24, doi:10.1016/j.tecto.2009.01.008.
- Özdemir, O., and D. J. Dunlop (2010), Hallmarks of maghemitization in low-temperature remanence cycling of partially oxidized magnetite nanoparticles, *J. Geophys. Res.*, *115*, B02101, doi:10.1029/2009JB006756.
- Pan, Y. X., R. X. Zhu, S. K. Banerjee, J. Gill, and Q. Williams (2000), Rock magnetic properties related to thermal treatment of siderite: Behavior and interpretation, *J. Geophys. Res.*, *105*, 783–794.
- Pei, J. L., Z. Z. Zhou, S. G. Dong, and L. Tang (2014a), Magnetic evidence revealing frictional heating from fault rocks in granites, *Tectonophysics*, *637*, 207–217.
- Pei, J. L., H. B. Li, H. Wang, J. L. Si, Z. M. Sun, and Z. Z. Zhou (2014b), Magnetic properties of the Wenchuan Earthquake Fault Scientific Drilling Project Hole-1 (WFSD-1), Sichuan Province, China, *Earth Planets Space*, *66*, 23, doi:10.1186/1880-5981-66-23.
- Pei, J. L., Z. Z. Zhou, H. B. Li, H. Wang, F. Liu, M. Sheng, and Y. Zhao (2016), New evidence of repeated earthquakes along Wenchuan earthquake fault zone [in Chinese], *Geol. China*, *43*(1), 43–55.
- Pittarello, L., G. Pennacchioni, and G. Di Toro (2012), Amphibolite-facies pseudotachylytes in Premosello metagabbro and felsic mylonites (Ivrea zone, Italy), *Tectonophysics*, *580*, 43–57.
- Roberts, A. P., Y. L. Cui, and K. L. Verosub (1995), Wap-waisted hysteresis loops: Mineral magnetic characteristics and discrimination of components in mixed magnetic systems, *J. Geophys. Res.*, *100*, 17,909–17,924.
- Shigetomi, M., and A. M. Lin (1999), Seismic events inferred from the layering structures of fault gouge and pseudotachylytes in the Nojima fault zone, Japan, *Struct. Geol. J. Tecton. Group Jpn.*, *43*, 33–42.
- Sibson, R. H. (1975), Generation of pseudotachylyte by ancient seismic faulting, *Geophys. J. R. Astron. Soc.*, *43*, 775–779.
- Sibson, R. H. (1977), Fault rocks and fault mechanisms, *J. Geol. Soc. London*, *133*, 191–214.
- Spray, J. G. (1992), A physical basis for the frictional melting of some rock-forming minerals, *Tectonophysics*, *204*, 205–221.
- Tanikawa, W., T. Mishima, T. Hirono, W. Soh, and S.-R. Song (2008), High magnetic susceptibility produced by thermal decomposition of core samples from the Chelungpu fault in Taiwan, *Earth Planet. Sci. Lett.*, *272*(1–2), 372–381.
- Tauxe, L., T. A. Mullender, and T. Pick (1996), Potbellies, wasp-waists, and superparamagnetism in magnetic hysteresis, *J. Geophys. Res.*, *101*, 571–583.
- Ujii, K., H. Yamaguchi, A. Sakaguchi, and S. Toh (2007), Pseudotachylytes in an ancient accretionary complex and implications for melt lubrication during subduction zone earthquakes, *J. Struct. Geol.*, *29*, 599–613.
- Verwey, E. J., P. W. Haayman, and F. C. Romeijn (1947), Physical properties and cation arrangement of oxides with spinel structures II. Electronic conductivity, *J. Chem. Phys.*, *15*, 181–187.
- Wang, H., H. B. Li, J. L. Si, Z. M. Sun, and Y. Huang (2014), Internal structure of the Wenchuan earthquake fault zone, revealed by surface outcrop and WFSD-1 drilling core investigation, *Tectonophysics*, *619–620*, 101–114.
- Wang, H., H. B. Li, C. Janssen, Z. M. Sun, and J. L. Si (2015), Multiple generations of pseudotachylyte in the Wenchuan fault zone and their implications for coseismic weakening, *J. Struct. Geol.*, *74*, 159–171.
- Xu, Z. Q., H. B. Li, and Z. L. Wu (2008), Wenchuan earthquake and scientific drilling [in Chinese], *Acta Geol. Sin.*, *82*(12), 1613–1622.
- Yang, T., J.-Y. Chen, H.-Q. Wang, and H.-Q. Jin (2012a), Rock magnetic properties of fault rocks from the rupture of the 2008 Wenchuan Earthquake, China and their implications: Preliminary results from the Zhaojiagou outcrop, Beichuan County (Sichuan), *Tectonophysics*, *530–531*, 331–341.
- Yang, T., J.-Y. Chen, H.-Q. Wang, and H.-Q. Jin (2012b), Magnetic properties of fault rocks from the Yingxiu-Beichuan fault: Constraints on temperature rise within the shallow slip zone during the 2008 Wenchuan Earthquake and their implications, *J. Asian Earth Sci.*, *50*, 52–60.
- Yang, T., J.-Y. Chen, X.-S. Yang, H.-Q. Wang, and H.-Q. Jin (2013), Differences in magnetic properties of fragments and matrix of breccias from the rupture of the 2008 Wenchuan earthquake, China: Relationship to faulting, *Tectonophysics*, *601*, 112–124.
- Yang, T., X. Yang, Q. Duan, J. Chen, and M. J. Dekkers (2016), Rock magnetic expression of fluid infiltration in the Yingxiu-Beichuan fault (Longmen Shan thrust belt, China), *Geochem. Geophys. Geosyst.*, *17*, 1065–1085, doi:10.1002/2015GC006095.
- Zhang, L., et al. (2017), Magnetic susceptibility of WFSD-2 borehole cores from the Longmenshan thrust belt and its implications for great seismic activity [in Chinese], *Chin. J. Geophys.*, *60*(1), 225–239, doi:10.6038/cjg20170119.
- Zhang, P. Z., X. W. Xu, X. Z. Wen, and Y. K. Ran (2008), Slip rates and recurrence intervals of the Longmen Shan active fault zone, and tectonic implications for the mechanism of the May 12 Wenchuan earthquake, 2008, Sichuan, China [in Chinese], *Chin. J. Geophys.*, *51*(4), 1066–1073.
- Zhang, W., H. B. Li, R. Huang, J. L. Si, D. L. Liu, Y. Li, H. Wang, G. Yang, and L. W. Sun (2012), Lithologic characteristics and fault zone structure revealed by No.2 hole cores of the Wenchuan Earthquake Fault Zone Scientific Drilling (WFSD-2) [in Chinese], *Geol. Bull. China*, *31*(8), 1201–1218.
- Zheng, Y., H. B. Li, Z. M. Sun, H. Wang, J. J. Zhang, C. L. Li, and Y. Cao (2016), New geochronology constraints on timing and depth of the ancient earthquakes along the Longmen Shan fault belt, eastern Tibet, *Tectonics*, *35*, 2781–2806, doi:10.1002/2016TC004210.